Available online at www.sciencedirect.com
SCIENCE DIRECT®
Bioelectrochemistry 60 (2003) 107–114
Bioelectrochemistry
www.elsevier.com/locate/bioelechem

Electrical energy required to form large conducting pores

John C. Neu[a], Kyle C. Smith[b], Wanda Krassowska[b,*]

[a] Department of Mathematics, University of California at Berkeley, Berkeley, CA, USA
[b] Department of Biomedical Engineering, Duke University, Durham, NC 27708, USA

Received 27 January 2003; received in revised form 2 May 2003; accepted 22 May 2003

Abstract

This study computes the contribution of the externally induced transmembrane potential to the energy of large, highly conductive pores. This work was undertaken because the pore energy formulas existing in the literature predict qualitatively different behavior of large pores: the original formula proposed by Abidor et al. in 1979 implies that the electrical force expanding the pore increases linearly with pore radius, while later extensions of this formula imply that this force decreases to zero for large pores. Starting from the Maxwell stress tensors, our study derives the formula for the mechanical work required to deform a dielectric body in an ionic solution with steady-state electric current. This formula is related to a boundary value problem (BVP) governing electric potentials and fields in a proximity of a pore. Computer simulations yield estimates of the electrical energy for pores of two different shapes: cylindrical and toroidal. In both cases, the energy increases linearly for pore radii above approximately 20 nm, implying that the electrical force expanding the pore asymptotes to a constant value for large pores. This result is different from either of the two energy formulas mentioned above. Our study traces the source of this disagreement to approximations made by previous studies, which are suitable only for small pores. Therefore, this study provides a better understanding of the energy of large pores, which is needed for designing pulsing protocols for DNA delivery.

Keywords: Electric field; Electroporation; Maxwell stress tensor; Pore energy; Pore expansion rate; DNA delivery

1. Introduction

Experiments conducted on artificial bilayers, suspensions of vesicles or cells and tissues have demonstrated that a large, externally induced transmembrane potential ($\Delta\phi_m$) causes a dramatic increase in the permeability of the membrane. This effect is usually explained in terms of pores, i.e., small holes in the membrane, whose creation and subsequent growth is facilitated by large $\Delta\phi_m$. In 1979, Abidor et al. proposed a theoretical explanation for the role of $\Delta\phi_m$ in electroporation. Specifically, $\Delta\phi_m$ decreases the energy of a pore by affecting the capacitive energy stored in the membrane. In their original paper [1], this electrical contribution to the pore energy, U_E, was given by

$$U_E = -\frac{1}{2h}(\varepsilon_w - \varepsilon_m)(\Delta\phi_m)^2\pi r^2, \quad (1)$$

where h is the membrane thickness, ε_w and ε_m are permittivities of water and the membrane and r is the radius of a cylindrical pore. Formula (1) can be easily derived from the classical example of a dielectric slab sliding between the plates of a capacitor whose voltage is held constant [2,3]. Thus, formula (1) stipulates that both the membrane and the water filling the pore are purely dielectric and that the upper and lower surfaces of the membrane and the pore are kept at constant potentials that differ by $\Delta\phi_m$. Strictly speaking, these assumptions apply only to very small pores of negligible conductance.

Formula (1) was later extended by Pastushenko and Chizmadzhev [4] to account for the flow of current through a pore. Their formula for the energy of conducting pores,

$$U_E = -\frac{\pi}{h}(\varepsilon_w - \varepsilon_m)(\Delta\phi_m)^2\int_0^r \frac{r\,dr}{(1+\lambda)^2}, \quad (2)$$

accounts for the decrease of voltage difference across the pore: $\Delta\phi_m$ is divided between the pore resistance, R_p, and the "input resistance," $R_i = 1/(2\kappa r)$, where κ is the conductivity of the solution. The ratio $R_i/R_p \equiv \lambda$ appears in Eq. (2) and is computed according to the formula

$$\lambda = \frac{\pi r}{2h}\exp^{-\mu^0/kT}, \quad (3)$$

* Corresponding author. Tel.: +1-919-660-5105; fax: +1-919-660-5405.
E-mail address: wanda.krassowska@duke.edu (W. Krassowska).

1567-5394/03/$ - see front matter © 2003 Elsevier B.V. All rights reserved.
doi:10.1016/S1567-5394(03)00051-3

where $\mu^0 = e^2 P(\varepsilon_m/\varepsilon_w)/(r\varepsilon_m)$ is the Born energy of an ion, P is the Parsegian function [5], e is the elementary charge, k is Boltzmann constant and T is absolute temperature. Including μ^0 in the pore energy formula of Pastushenko and Chizmadzhev accounts for the interaction of ions with pore walls. This interaction has been further refined by Barnett and Weaver [6], who amended Eq. (3) by introducing the steric hindrance factor.

One needs to recognize that formulas (1) and (2) apply only to small pores, whose radii are much less than the membrane thickness. This focus on the energy of small pores came from the need to explain electroporation experiments that use high-voltage, short pulses to create a large number of pores with radii not substantially larger than 1 nm [7,8]. However, when electroporation is used for DNA delivery, it usually involves low voltage and long pulses [9,10]. The exact mechanism of DNA uptake is still debated. Some researchers postulate that DNA uptake relies on the DNA–membrane interactions, possibly involving several small pores [11–13]. On the other hand, an observation that low-voltage, long pulses create fewer but larger pores [14,15] suggests that pulses used for DNA delivery may create pores whose radii are tens of nanometers, i.e., large enough to allow the passage of a DNA molecule. For such pores, the interaction of ions with the pore walls, which features prominently in Eq. (2), is not relevant; it is more important to correctly represent the growth rate of very large pores. This growth rate is proportional to the radial force, which can be computed by differentiating pore energy with respect to radius r. Here, the two existing estimates differ: Eq. (1) predicts that the electrical component of the growth rate increases linearly with radius, while Eq. (2) predicts that it decays to zero as $1/r$. Thus, there is a need to reexamine the contribution of the transmembrane potential $\Delta\phi_m$ to the pore energy and to develop a theory that applies to large conductive pores.

This study derives such a theory from first principles. Starting from the Maxwell stress tensor, Section 2 derives the formula for the rate of mechanical work required to deform a dielectric body in an ionic solution with steady-state electric current. Section 3 applies this general formula to a pore and derives the formula for the pore energy for two pore geometries: cylindrical and toroidal. Section 4 presents the results of computer simulations, in which the electrical energies calculated for cylindrical and toroidal pores are compared with the energies computed from the original formula (1) of Abidor et al. [1] and from its later extension (Eq. (2)) of Pastushenko and Chizmadzhev [4] and Barnett and Weaver [6].

2. Mechanical work required to deform dielectric bodies in dielectric/conductive fluid

Consider a system consisting of a positive electrode E_+ and a negative electrode E_- separated by a dielectric/conductive fluid Ω with permittivity ε_w and conductivity κ, which contains purely dielectric bodies M with permittivity ε_m (Fig. 1). Electrodes E_+ and E_- are connected to a battery, which maintains a constant voltage difference $\Delta\phi_m$ between E_+ and E_-. The electric potential in the fluid is denoted by ψ and governed by the following boundary value problem (BVP):

$$\nabla^2\psi = 0 \text{ in } \Omega, \tag{4}$$

$$\psi = \Delta\phi_m \text{ on } E_+, \quad \psi = 0 \text{ on } E_-, \quad \psi \to 0 \text{ at } \infty, \tag{5}$$

$$\hat{n}\cdot\nabla\psi = 0 \text{ on } \partial M, \tag{6}$$

where ∂M denotes the fluid–body interface. The potential ψ is completely determined by Eqs. (4)–(6). Given ψ, the potential ϕ in the dielectric body M can be computed from the following BVP:

$$\nabla^2\phi = 0 \text{ in } M, \tag{7}$$

$$\phi = \psi \text{ on } \partial M. \tag{8}$$

Electric fields in dielectric media give rise to forces described by the Maxwell stress tensor [16]. Specifically, the force per unit area (stress) exerted by the fluid Ω upon the body M is

$$\mathbf{p}_w = -\mathbf{T}_w\hat{n} \tag{9}$$

where $\hat{n}$ is the outward normal on ∂M and $\mathbf{T}_w$ is the Maxwell stress tensor defined as

$$\mathbf{T}_w \equiv \varepsilon_w\left(\frac{1}{2}|\nabla\psi|^2\mathbf{I} - \nabla\psi\otimes\nabla\psi\right) \tag{10}$$

with $\mathbf{I}$ denoting the identity matrix [16]. Eq. (9) assumes a quasistatic situation with negligible velocity field (i.e., the fluid is essentially motionless). Similarly, the dielectric

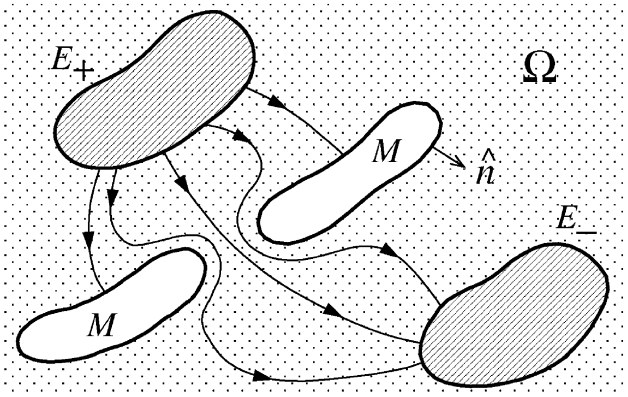

Fig. 1. Dielectric body M in a dielectric/conductive fluid Ω. E_+ and E_- are metal electrodes kept at constant potentials that differ by $\Delta\phi_m$.

body exerts stress on the fluid with electric component $-\mathbf{T_m}(-\hat{n})=\mathbf{T_m}\hat{n}$, where

$$\mathbf{T_m}\equiv\varepsilon_m\left(\frac{1}{2}\,|\,\nabla\phi\,|^2\mathbf{I}-\nabla\phi\otimes\nabla\phi\right) \tag{11}$$

is the Maxwell stress tensor in the body. The stress owing to all other mechanical properties of the body is denoted by **f**. Thus, the total stress exerted by the body M on the fluid Ω is

$$\mathbf{p_m}=\mathbf{T_m}\hat{n}+\mathbf{f}. \tag{12}$$

The condition of local mechanical equilibrium on the interface dictates that stresses given by Eqs. (9) and (12) are equal and opposite. Thus,

$$\mathbf{f}=(\mathbf{T_w}-\mathbf{T_m})\hat{n}. \tag{13}$$

Given the electrical state of the system as specified by ψ and ϕ, Eq. (13) determines the necessary mechanical force exerted by the body to maintain equilibrium. When the body M deforms with velocity v normal to its surface, the body does mechanical work at the rate [17]

$$\dot{U}_E=\int_{\partial M}(\mathbf{f}\cdot\hat{n})v\mathrm{d}a=\int_{\partial M}\hat{n}\cdot(\mathbf{T_w}-\mathbf{T_m})\hat{n}v\mathrm{d}a$$
$$=\int_{\partial M}p_E v\mathrm{d}a, \tag{14}$$

where p_E denotes the net electric stress normal to the interface ∂M,

$$p_E=\hat{n}\cdot(\mathbf{T_w}-\mathbf{T_m})\hat{n}. \tag{15}$$

Using the definitions of stress tensors (Eqs. (10) and (11)), the stress p_E can be expressed in terms of local electric fields,

$$p_E=\frac{1}{2}\left[\varepsilon_w e_\parallel^2-\varepsilon_m E_\parallel^2-\left(\frac{d_\perp^2}{\varepsilon_w}-\frac{D_\perp^2}{\varepsilon_m}\right)\right], \tag{16}$$

where $e_\parallel$ and $E_\parallel$ are the tangential components of the electric field evaluated in fluid Ω and body M, respectively. Likewise, $d_\perp\equiv\varepsilon_w e_\perp$ and $D_\perp\equiv\varepsilon_m E_\perp$ are normal components of the dielectric flux evaluated in Ω and M, respectively.

From the continuity of potential condition (6), $\psi=\phi$ on ∂M, so $e_\parallel$ can be replaced by $E_\parallel$ in Eq. (16). However, dielectric fluxes $d_\perp$ and $D_\perp$ are not equal: the macroscopic BVPs described by Eqs. (4)–(6) and Eqs. (7) and (8) imply that there is a surface charge equal to $(d_\perp-D_\perp)$ on ∂M. On a microscopic level, this surface charge takes the form of the imbalance in the densities of positive and negative ions in a thin layer of fluid near the interface, which is described by a nonequilibrium but steady-state extension of the Poisson–Boltzmann theory [18]. This layer will cause the actual values of ψ on the interface to differ from those calculated from Eqs. (4)–(6); in Fig. 2, this microscopic-level distribution of potential is denoted by ψ' and shown with the dashed line. Because of the boundary condition (8), potential in the body will also differ (see ϕ' in Fig. 2).

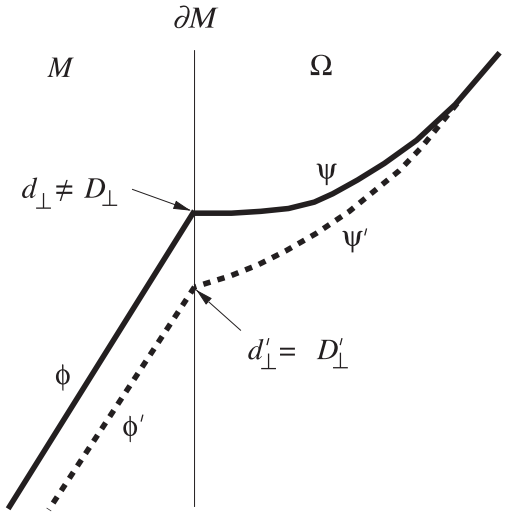

Fig. 2. Sketch of the macroscopic (solid line) and microscopic (dashed line, primed symbols) potentials at the body–fluid interface ∂M.

Note that the dielectric flux computed from microscopic potentials ψ' and ϕ' is continuous across ∂M: $d'_\perp=D'_\perp$. Since the ionic layer is thin (the Debye length for physiological solutions is below 1 nm [19]), its effect on ϕ and its gradient is small and can be neglected. Thus, microscopic dielectric flux $D'_\perp\approx D'_\perp$, with $D_\perp$ computed from the macroscopic BVP (Eqs. (7) and (8)). Consequently, $d_\perp$ can be replaced by $D_\perp$ in Eq. (16). When $D_\perp$ is expressed in terms of the normal electric field $E_\perp$, we obtain the final expression for the electric stress

$$p_E=\frac{1}{2}(\varepsilon_w-\varepsilon_m)\left(E_\parallel^2+\frac{\varepsilon_w}{\varepsilon_m}E_\perp^2\right), \tag{17}$$

in which $E_\parallel$ and $E_\perp$ are evaluated on the dielectric body side of the interface ∂M.

3. Energy required to form a pore

Formula (14) for the rate of mechanical work done by the dielectric body in the dielectric/conductive fluid in the presence of electric field can be used to derive the formula for the electrical energy required to form a pore. Here, we will consider pores of two geometries: cylindrical and toroidal (Fig. 3). Large conducting pores are better approximated by the toroidal geometry, as their interior surface S is lined with the hydrophilic heads of the lipid molecules [20]. Cylindrical pores are considered here to facilitate comparison with previous estimates of the pore energy in Eqs. (1) and (2), which were derived assuming this geometry.

Assuming that the bilayer cannot be compressed, velocity v in Eq. (14) is strictly radial, and the integral over ∂M

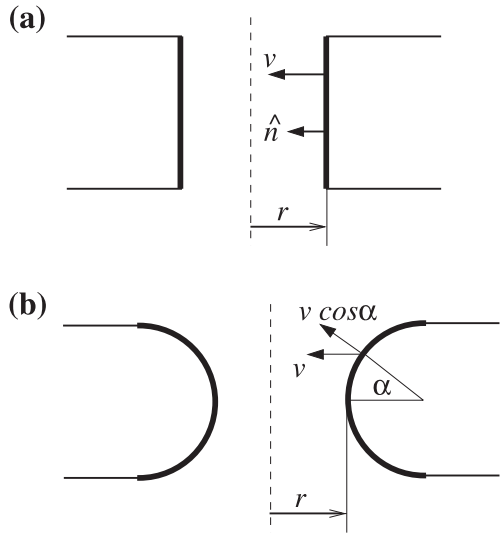

Fig. 3. Pore models with (a) cylindrical and (b) toroidal geometry of their inside surface. Heavy line outlines the interior surface of the pore, S, over which the integration in formulas (20) and (21) is performed.

needs to be performed only over the interior surface of the pore, S. For a cylindrical pore,

$$v = -\frac{\mathrm{d}r}{\mathrm{d}t}, \tag{18}$$

where the minus sign arises because v in Eq. (14) is in the direction of the normal vector $\hat{n}$, which points into the pore (Fig. 3). Introducing Eq. (18) into Eq. (14), performing integration with respect to time and changing the variable of integration from t to r, one obtains the expression for the pore energy U_{E},

$$U_{\mathrm{E}}(r) = -\int_0^r F(r)\mathrm{d}r, \tag{19}$$

where $F(r)$ is the total electrical force expanding the pore, computed by integrating the stress p_{E} over the pore surface,

$$F(r) = \int_S p_{\mathrm{E}}\mathrm{d}a. \tag{20}$$

For a toroidal pore, the energy is given by the same expression (19), but the computation of the radial force F must account for the shape of the pore,

$$F(r) = \int_S p_{\mathrm{E}}\cos\alpha\,\mathrm{d}a, \tag{21}$$

where angle α is measured as shown in Fig. 3b.

It is easily seen that in a limit of a small cylindrical pore, our formula for pore energy (Eq. (19)) reduces to formula (1) given by Abidor et al. As $r \to 0$ and the pore becomes essentially nonconducting, the voltage drop across the pore becomes equal to $\Delta\phi_{\mathrm{m}}$ and the BVPs Eqs. (4)–(6) and Eqs. (7) and (8) become one-dimensional, with both ψ and ϕ varying linearly from 0 on the bottom surface of the pore to $\Delta\phi_{\mathrm{m}}$ on the top surface. Hence, local electric fields are $E_{\parallel} = -\Delta\phi_{\mathrm{m}}/h$ and $E_{\perp} = 0$, and the electric stress evaluated from Eq. (17) is

$$p_{\mathrm{E}} = \frac{1}{2}(\varepsilon_{\mathrm{w}} - \varepsilon_{\mathrm{m}})\frac{(\Delta\phi_{\mathrm{m}})^2}{h^2}. \tag{22}$$

Consequently, the radial force F, evaluated from Eq. (20) is

$$F(r) = \frac{1}{h}(\varepsilon_{\mathrm{w}} - \varepsilon_{\mathrm{m}})(\Delta\phi_{\mathrm{m}})^2\pi r, \tag{23}$$

which, integrated in r according to Eq. (19), yields formula (1) for the pore energy of Abidor et al.

4. Results of numerical simulations

The theory developed in the two previous sections was applied to cylindrical and toroidal pores (Fig. 3), whose radius r varied between 0.1 and 100 nm. Taking advantage of rotational symmetry, potentials were expressed in cylindrical coordinates as functions of radius ρ, measured from the pore axis, and z, measured from the midplane of the membrane. Assuming that electrodes E_+ and E_- are very far from the pore, the general boundary conditions in Eq. (5) were replaced by

$$\begin{aligned} &\psi \to \Delta\phi_{\mathrm{m}} \text{ as } \sqrt{\rho^2+z^2} \to \infty,\ z > 0,\\ &\text{and } \psi \to 0 \text{ as } \sqrt{\rho^2+z^2} \to \infty,\ z < 0. \end{aligned} \tag{24}$$

Electric potentials and fields were computed using the finite element program PDEase from Macsyma, [21]. Only the upper half of the pore was represented in the model; the boundary condition $\psi = \phi = \Delta\phi_{\mathrm{m}}/2$ was used on the $z = 0$ plane. To develop a finite element model, the pore had to be enclosed in a finite domain, a cylinder of the radius $\rho_{\max}$ and height $z_{\max}$. The outer boundary of this cylinder was assigned the Dirichlet boundary condition,

$$\psi = \Delta\phi_{\mathrm{m}} - \frac{\Delta\phi_{\mathrm{m}}}{\pi}\sin^{-1}\left(\frac{2a}{\sqrt{(\rho-a)^2+z^2}+\sqrt{(\rho+a)^2+z^2}}\right) \tag{25}$$

on the upper end of the cylinder ($z = z_{\max}$) and on its side surface ($\rho = \rho_{\max}$). Expression (25) was adopted from the formula for the potential generated by a charged, conducting disk given by Jackson [22]. In computations, both $\rho_{\max}$ and $z_{\max}$ were equal to 20 × the pore radius. Other parameters were as follows: conductivity $\kappa = 2$ S/m, permittivities $\varepsilon_{\mathrm{w}} = 80\varepsilon_0$ and $\varepsilon_{\mathrm{m}} = 2\varepsilon_0$, where ε_0 was the permittivity of vacuum, 8.85×10^{-12} F/m, and membrane thickness $h = 5$ nm. All results were obtained with the transmembrane potential away from the pore $\Delta\phi_{\mathrm{m}} = 1$ V.

After the PDEase program computed the distribution of potentials ψ in the water and ϕ in the membrane, it determined local electric fields normal and tangential to the pore surface using potential ϕ within the *membrane*. These local fields were combined according to Eq. (17) to obtain the electric stress p_E. Next, PDEase integrated p_E over the pore surface of obtain the total radial force F, using Eq. (20) for cylindrical pores and Eq. (21) for toroidal pores. This procedure was repeated for pores of several different radii r, yielding force F as a function of r. Finally, $F(r)$ was integrated in r according to Eq. (19), determining the electrical component of the pore energy, $U_E(r)$.

Fig. 4 compares radial force $F(r)$ calculated as outlined above for cylindrical and toroidal pores. Also included are the force estimates obtained by differentiating the pore energy formulas of Abidor et al. (Eq. (1)) and of Pastushenko and Chizmadzhev (Eq. (2)). For small radii (Fig. 4b), all curves are very close, although the force for toroidal pores is larger than that for cylindrical pores. Hence, pores with toroidal surface are expected to grow at a faster rate

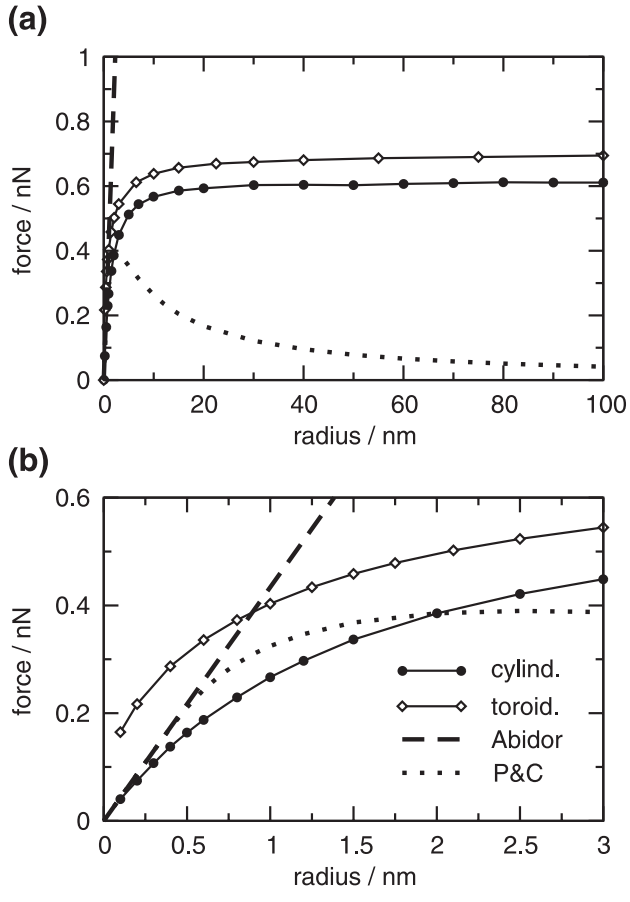

Fig. 4. Radial force F as a function of the pore radius at the transmembrane potential $\Delta\phi_m = 1$ V. Panel (b) shows F for very small radii. The labels are 'cylind.'–numerical solution for cylindrical pores, 'toroid.'–numerical solution for toroidal pores, 'Abidor'–force computed from formula (1) of Abidor et al., and 'P&C'–force computed from formula (2) of Pastushenko and Chizmadzhev (including modifications by Barnett and Weaver as described in Ref. [20]).

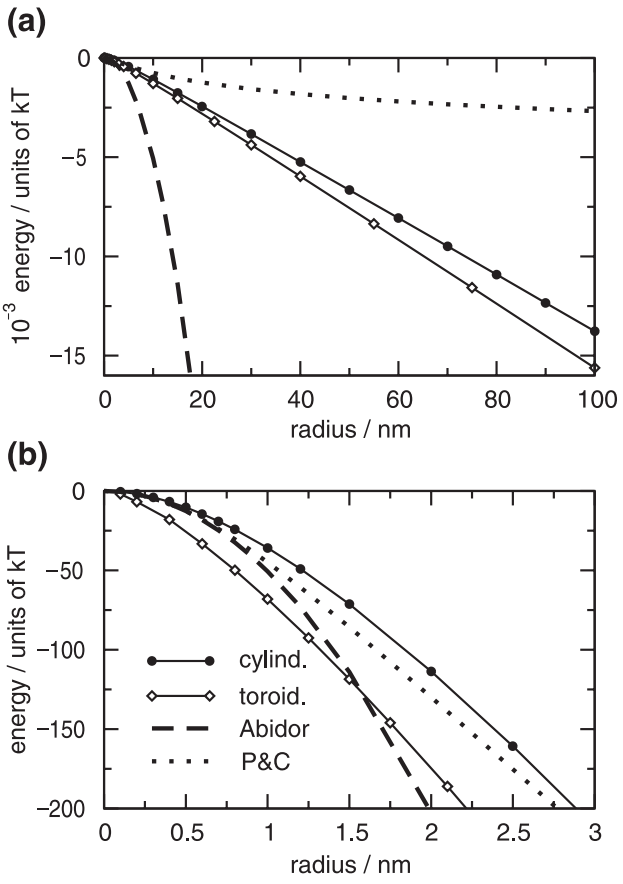

Fig. 5. Electrical component of the pore energy U_E as a function of the pore radius at the transmembrane potential $\Delta\phi_m = 1$ V. Panel (b) shows U_E for very small radii. The labels are as in Fig. 4.

than cylindrical pores. For large radii (Fig. 4a), the force computed from the Abidor's formula grows linearly with pore radius, the force computed numerically for both cylindrical and toroidal pores levels off at a constant value, and the force computed from the Pastushenko and Chizmadzhev's formula decreases with pore radius like $1/r$.

Fig. 5 compares pore energies $U_E(r)$ for the same four cases. For small pores (Fig. 5b), there is little difference between these four estimates. For large radii (Fig. 5a), the energy computed from the Abidor's formula grows (in the negative direction) quadratically with pore radius, the energy computed numerically for both cylindrical and toroidal pores grows linearly and the energy computed from the Pastushenko and Chizmadzhev's formula also grows but only at a logarithmic rate.

We found it convenient to approximate the numerical results with analytical expressions. Hence, for cylindrical pores, we use the following approximation for the radial force:

$$F(r, \Delta\phi_m) = \frac{F_{max}}{1 + r_h/r}(\Delta\phi_m)^2 \quad (26)$$

with $F_{max} = 6.38 \times 10^{-10}$ N/V^2 and $r_h = 1.466 \times 10^{-9}$ m. In the limit of very small pores, formula (26) reduces to

$F(r,\Delta\phi_m) \sim (F_{max}/r_h)r(\Delta\phi_m)^2$, which is consistent with the force (Eq. (23)) computed by differentiating the energy (Eq. (1)) given by Abidor et al., provided that F_{max} and r_h are chosen so that $(F_{max}/r_h)=(\varepsilon_w-\varepsilon_m)\pi/h$. This condition is satisfied for the parameters given above. For toroidal pores, the approximation for the force is

$$F(r,\Delta\phi_m)=\frac{F_{max}}{1+r_h/(r+r_t)}(\Delta\phi_m)^2 \quad (27)$$

with $F_{max}=6.9\times10^{-10}$ N/V^2 $r_h=0.95\times10^{-9}$ m, and $r_t=0.23\times10^{-9}$ m.

5. Discussion

This study has developed a method for estimating the electrical component of pore energy that is applicable to large conducting pores. In the limit of small pore radii, the pore energy computed in this study agrees with the pore energy estimates proposed previously (Fig. 5b). However, as the pore radius increases, large differences between our results and previous ones emerge (Fig. 5a), and they have significant implications for the growth of large pores. The original formulation of pore energy of Abidor et al. implies that the radial force F increases linearly with the pore radius (Fig. 4a). Thus, the contribution of the transmembrane potential to the pore growth rate increases with the pore radius. The later refinement of the pore energy formula by Pastushenko and Chizmadzhev [4] and by Barnett and Weaver [6] leads to F decreasing to zero, implying the decrease in the contribution of the transmembrane potential to the growth rate of large pores. Our estimate falls between these two: the force F levels off for large pore radii (above 20 nm) implying that the electrical contribution to the growth rate of large pores is constant, regardless of the pore radius.

The reason for the discrepancy between our results and those of Abidor et al. [1] is easy to see. Formula (1) assumes that the pore maintains a constant voltage difference equal to that of the intact membrane ($\Delta\phi_m$ in Fig. 6). This assumption is satisfied only for very small pores that are essentially nonconducting. Indeed, as the pore radius decreases below 0.5 nm, our results for cylindrical pores coincide with those of Abidor et al. (Figs. 4b and 5b).

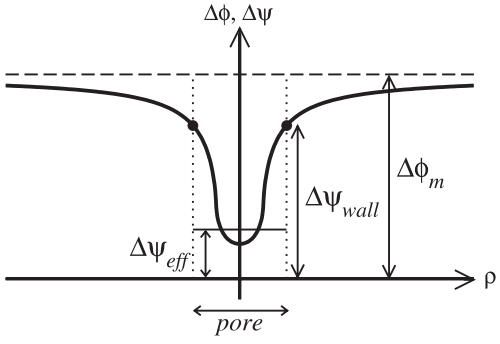

Fig. 6. Potential difference across the membrane ($\Delta\phi$) and across the pore ($\Delta\psi$). This plot assumed pore radius $r=10$ nm and transmembrane potential away from the pore $\Delta\phi_m=1$ V.

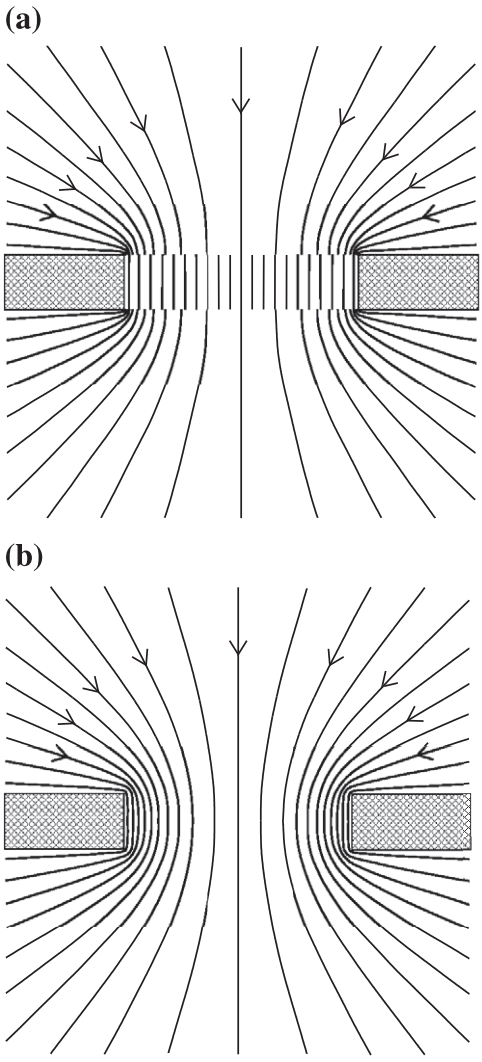

Fig. 7. Lines of electric field inside and in the proximity of a pore. Panel (a) visualizes the approximation used by Pastushenko and Chizmadzhev [4]. Panel (b) corresponds to the numerical solution of the full BVP (Eqs. (4), (6) and (24)).

The reason for the discrepancy between our results and the estimate (2) developed by Pastushenko and Chizmadzhev [4] is more subtle. On the surface of it, their model is very similar to ours: both models assume a dielectric membrane in a dielectric/conductive fluid and use Maxwell stress tensors to evaluate the force expanding the pore. Pastushenko and Chizmadzhev neglect the contribution of the normal component of the electric field. However, this simplification is no consequence: in our calculations, $E_\perp$ contributes only about 0.5% to the total force. The real difference is the replacement of the full

boundary value problem (Eqs. (4), (6) and (24)) by a simplified one that admits the analytical solution. Specifically, Pastushenko and Chizmadzhev assumed that the potential ψ was spatially uniform across the top and bottom surface of a cylindrical pore, so that the electric field in the pore was uniform and axial. The value of the "effective" potential difference across the pore, $\Delta\psi_{\mathrm{eff}}$ (Fig. 6), was chosen so that the current flowing though the pore is the same as the current entering the conducting disk kept at a constant potential equal to $(\Delta\phi_{\mathrm{m}} - \Delta\psi_{\mathrm{eff}})/2$ (using the notation of our study). Thus, the potential in the fluid outside the pore was related to the potential established by a charged, conducting disk (Eq. (25)). As seen in Fig. 7, the approximate solution of Pastushenko and Chizmadzhev is substantially different from the solution of the full BVP: assuming constant ψ across the top and bottom of the pore results in a uniform spacing of the electric field lines within the pore (Fig. 7a). In contrast, electric field lines of the full BVP naturally concentrate near the pore walls (Fig. 7b), indicating the increased magnitude of the electric field in this area.

In the approximation of Pastushenko and Chizmadzhev, the spatially uniform potential across the pore $\Delta\psi_{\mathrm{eff}} \sim \Delta\phi_{\mathrm{m}}h/r$ for $r \gg h$. Hence, in formula (17) for electric stress, $E_{\parallel} \sim 1/r$ and $p_{\mathrm{E}} \sim 1/r^2$. Consequently, the integral of p_{E} over the pore walls scales like $(1/r^2)$, $r = 1/r$, so that the radial force expanding the pores is $F \sim 1/r$ for $r \gg h$ (Fig. 4, dotted line). In the full BVP problem used in our study, the potential across the pore is not spatially uniform: it is largest next to the pore wall ($\Delta\psi_{\mathrm{wall}}$ in Fig. 6). It is evident that the electric field $E_{\parallel}$ that is used to compute stress tensors should be evaluated using potential $\Delta\psi_{\mathrm{wall}}$ *on the interior surface of the pore* and not the "effective" constant potential $\Delta\psi_{\mathrm{eff}}$ used by Pastushenko and Chizmadzhev. The potential $\Delta\psi_{\mathrm{wall}}$ also decreases to zero as $r \to \infty$, but at a much slower rate: singular perturbation analysis of BVPs Eqs. (4)–(6) and Eqs. (7) and (8) indicates that $\Delta\psi_{\mathrm{wall}} \sim \Delta\phi_{\mathrm{m}}\sqrt{h/r}$ for $r \gg h$. Hence, $E_{\parallel} \sim 1/\sqrt{r}$, the electric stress $p_{\mathrm{E}} \sim 1/r$ and the integral of p_{E} over the pore walls scales like $(1/r)$, $r = 1$, resulting in the force expanding the pores that asymptotes to a constant value as $r \to \infty$. This estimate confirms the numerical results given in Fig. 4. Therefore, there is reason to believe that our study gives a more realistic estimate of the electrical contribution to the pore growth rate and the pore energy than the estimates proposed to date.

The theory derived here is quite general and can be applied to any experimental conditions. However, to form a complete model, the formula for the electrical force, Eqs. (26) or (27), must by supplemented by the formula for the mechanical energy of the pore, the governing equation for the pore creation and evolution, and an ordinary or partial differential equation describing the behavior of the transmembrane potential, $\Delta\phi_{\mathrm{m}}$. The equation for $\Delta\phi_{\mathrm{m}}$ will determine the experimental setup that the model represents. Hopefully, better understanding of the electrical energy of large pores provided by our study will enable the use of models to design or optimize pulsing protocols for DNA delivery.

Acknowledgements

Supported in part by the National Science Foundation Grant BES-0108408.

References

[1] I.G. Abidor, V.B. Arakelyan, L.V. Chernomordik, Y.A. Chizmadzhev, V.F. Pastushenko, M.R. Tarasevich, Electric breakdown of bilayer lipid membranes: I. Main experimental facts and their qualitative discussion, Bioelectrochem. Bioenerg. 6 (1979) 37–52.

[2] R.P. Feynman, R.B. Leighton, M. Sands, The Feynman Lectures on Physics, vol. II, Addison-Wesley, Reading, MA, 1963, pp. 7–8, ch. 10.

[3] R. Plonsey, R.E. Collin, Principles and Applications of Electromagnetic Fields, McGraw-Hill, New York, 1961, pp. 106–111.

[4] V.F. Pastushenko, Y.A. Chizmadzhev, Stabilization of conducting pores in BLM by electric current, Gen. Physiol. Biophys. 1 (1982) 43–52.

[5] V.A. Parsegian, Energy of an ion crossing dielectric membrane: solution to four relevant electrostatic problems, Nature (1969) 844–846.

[6] A. Barnett, J.C. Weaver, Electroporation: a unified, quantitative theory of reversible electrical breakdown and mechanical rupture in artificial planar bilayer membranes, Bioelectrochem. Bioenerg. 25 (1991) 163–182.

[7] R.W. Glaser, S.L. Leikin, L.V. Chernomordik, V.F. Pastushenko, A.I. Sokirko, Reversible electrical breakdown of lipid bilayers: formation and evolution of pores, Biochim. Biophys. Acta 940 (1988) 275–287.

[8] S. Kakorin, E. Neumann, Ionic conductivity of electroporated lipid bilayer membranes, Bioelectrochemistry 56 (2002) 163–166.

[9] M.-P. Rols, J. Teissié, Electropermeabilization of mammalian cells to macromolecules: control by pulse duration, Biophys. J. 74 (1998) 1415–1423.

[10] J. Gehl, L.M. Mir, Determination of optimal parameters for in vivo gene transfer by electroporation, using a rapid in vivo test for cell permeabilization, Biochem. Biophys. Res. Comm. 261 (1999) 377–380.

[11] V.A. Klenchin, S.I. Sukharev, S.M. Serov, L.V. Chernomordik, Y.A. Chizmadzhev, Electrically induced DNA uptake by cells is a fast process involving DNA electrophoresis, Biophys. J. 60 (1991) 804–811.

[12] S.I. Sukharev, V.A. Klenchin, S.M. Serov, L.V. Chernomordik, Y.A. Chizmadzhev, Electroporation and electrophoretic DNA transfer into cells. The effect of DNA interaction with electropores, Biophys. J. 63 (1992) 1320–1327.

[13] E. Neumann, S. Kakorin, I. Tsoneva, B. Nikolova, T. Tomov, Calcium-mediated DNA adsorption to yeast cells and kinetics of cell transformation by electroporation, Biophys. J. 71 (1996) 868–877.

[14] S.A. Freeman, M.A. Wang, J.C. Weaver, Theory of electroporation of planar bilayer membranes: predictions of the aqueous area, change in capacitance, and pore–pore separation, Biophys. J. 67 (1994) 42–56.

[15] R. Vanbever, U.F. Pliquett, V. Préat, J.C. Weaver, Comparison of the effects of short, high-voltage and long, medium voltage pulses on skin electrical and transport properties, J. Controlled Release 69 (1999) 35–47.

[16] L.D. Landau, E.M. Lifshitz, L.P. Pitaevskii, Electrodynamics of Continuous Media, 2nd ed., Landau and Lifshitz Course of Theoretical Physics, vol. 8, Pergamon, Oxford, UK, 1984, pp. 59–67.

[17] A.G. Hansen, Fluid Mechanics, Wiley, New York, NY, 1967, pp. 122–124.
[18] J. Israelachvili, Intermolecular and Surface Forces, 2nd ed., Academic Press, London, UK, 1992, pp. 213–223.
[19] D. Eisenberg, D. Crothers, Physical Chemistry with Applications to the Life Sciences, The Benjamin/Cummings Publishing, Menlo Park, CA, 1979, p. 357.
[20] J.C. Weaver, Y.A. Chizmadzhev, Theory of electroporation: a review, Bioelectrochem. Bioenerg. 41 (1996) 135–160.
[21] PDEase, Finite element analysis for partial differential equations, Reference Manual, Tutorial, Handbook of Demonstrations, 3rd ed., Macsyma, Arlington, MA, 1998.
[22] J.D. Jackson, Classical Electrodynamics, Wiley, New York, NY, 1962, pp. 89–93.